Microelectronic Engineering 241 (2021) 111547

Contents lists available at ScienceDirect

Microelectronic Engineering

journal homepage: www.elsevier.com/locate/mee

Research paper

High winding ratio, high frequency, ultracompact step-up transformers with laminated metallic magnetic cores

Tao Zhang *, Mark G. Allen

Department of Electrical and Systems Engineering, University of Pennsylvania, Philadelphia, PA 19104, USA

ARTICLE INFO

Keywords:
High winding ratio
Laminated permalloy cores
Sequential multilayer electrodeposition
Surface tension-driven self-assembly
Ultracompact step-up transformers

ABSTRACT

The development and characterization of step-up transformers with high winding ratios and laminated metallic magnetic cores for MHz-range step-up transformers used in DC-DC power converters is presented. The use of metallic magnetic cores with higher saturation flux density than traditional ferrites offers the possibility of reducing the physical size of the transformers. Core eddy currents are suppressed by forming the magnetic cores in a sequential electrodeposition process through toroidal lithographic molds, followed by self-assembly. This approach results in relatively thick magnetic cores (in the hundreds of microns range), comprised of many individual laminations with micron-scale thicknesses. Transformers were formed by manual winding of primary and secondary coils on these cores. The resultant transformers, with typical dimensions in the cubic millimeter range, exhibited primary and secondary inductances in the microhenry and hundreds of microhenry ranges, respectively. Typical transformer coupling coefficients were in the range 0.85–0.95. The transformers exhibited expected voltage step-up ratios as high as 10:1 at typical operation frequencies of 1–2 MHz. These ultracompact devices exhibit up to seven times higher inductance per unit volume and five times higher inductance per weight than typical commercial coupled inductors, and show promise for use in space-constrained electronic systems.

1. Introduction

The rapid development of information and communications technology is driving portable electronic devices toward both miniaturization and functional diversity. These trends are placing increasing demand on both the performance and size of the power conversion systems within these devices [1–5]. Much effort has gone toward reducing the physical size of switched DC-DC converters; the passive components such as transformers and inductors have been particularly targeted, since these elements typically comprise the largest volume fractions of the converters [6–10]. In addition to increasing converter switching frequency, which reduces the size requirement of the passive components, the utilization of new magnetic core materials such as advanced ferrites and metallic alloys have been studied to shrink the size of transformers and inductors [11–14].

Compared to ferrites, metallic alloys (e.g., permalloy, CoZrRe) are particularly attractive options for use in magnetic cores due to their relatively high saturation flux density. As shown in Table 1, metallic alloys have saturation flux density of 1–2 Tesla, several times higher than that of ferrites. As the achievable energy density from a magnetic core is linearly proportional to the square of saturation flux density [7], the volume of transformers and inductors can be further reduced with utilization of metallic alloys in magnetic cores. For instance, stacked spiral type transformers using permalloy as the core material were reported by Park et al. [15]. Solenoid type magnetic thin-film transformers with permalloy core material were fabricated by Yun et al. [16]. Moreover, solenoid type transformers utilizing ternary CoZrRe amorphous magnetic core films were developed by Mino et al. [17]. However, the resistivity of metallic alloys are orders of magnitude lower than that of ferrites (shown in Table 1). These transformers had to use magnetic thin films as their core materials (with core thicknesses limited to a few microns) for MHz frequency operation, since these electrically conducting materials can suffer from significant eddy current loss within the cores when the thickness of magnetic cores is larger than the skin depth of the materials. Hence, the inductance of these transformers is typically relatively low ($\leq$1 μH), potentially limiting their use in higher power applications.

To overcome this limitation, laminated magnetic cores have been proposed. Such cores can be achieved, for example, by repeated sequential sputtering of magnetic and insulating material to form a

* Corresponding author.
E-mail address: taozhan@seas.upenn.edu (T. Zhang).

https://doi.org/10.1016/j.mee.2021.111547
Received 24 December 2020; Received in revised form 2 March 2021;
Available online 27 March 2021

Table 1
Properties of typical magnetic and winding materials used in transformers.

Properties	Magnetic materials	
	Ferrite [22–24]	Metallic alloys [25–29]
Flux density B_s (T)	<0.5	1–2
Relative permeability μ_r	<100	>150
Resistivity ρ_m (Ω·m)	$>10^{-3}$	$<10^{-7}$
	Winding Materials	
	Copper	Aluminum
Mass density ρ (g/cm^3)	8.96	2.7

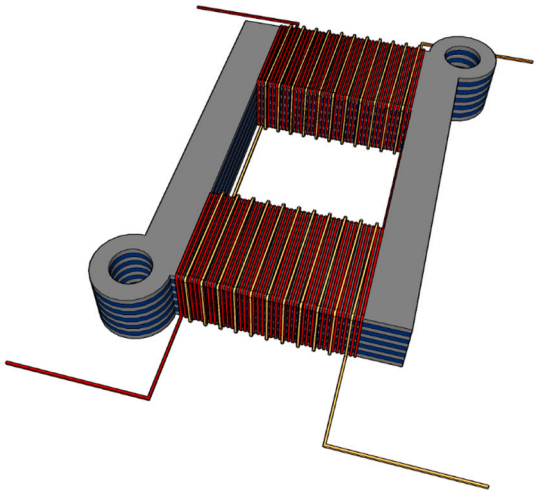

Fig. 1. Schematic view of a transformer with laminated magnetic core (yellow: primary coil; red: secondary coil). The core comprises a stack of individual magnetic lamination sheets with a closed rectangular flux path. Between each magnetic lamination is an electrical insulation layer. The ring-like features at diagonal ends of the core assist in lamination self-assembly.

laminated stack, in which eddy currents are suppressed [18,19]. Although individual laminations with thicknesses that suppress eddy currents can be achieved in this manner, it is challenging to achieve large total thicknesses (i.e., a large number of laminations) due to fabrication limitations such as film stress and processing time. In this work, laminated magnetic cores were fabricated by employing the technique of automated sequential multilayer electrodeposition and surface tension-driven self-assembly previously developed by our group for inductors [20,21]. To further reduce the weight of the transformers, aluminum was investigated as the winding material since it has lower mass density than copper (shown in Table 1); this strategy can be particularly effective in the secondary winding of step-up transformers, which typically supply high voltage and low current. Transformers with various designs based on these cores were fabricated and compared on the basis of inductance, resistance, coupling coefficient, voltage transformation ratio, and saturation current. The inductance density of these devices was compared with commercial transformers to demonstrate the compactness achievable using this approach.

2. Transformer design

To illustrate the utility of laminated magnetic core technology, rectangular closed loop laminated magnetic core transformers with multi-level, high turn ratio windings were designed and fabricated. The closed loop geometry was selected as it is not only the most efficient flux guide for transformer magnetic coupling [30], but also to exploit the potential for high inductance with this geometry [31]. Further, since a new transformer core approach is being evaluated, the use of the well-established equations for closed loop structures provides a relatively straightforward approach to both design and analyze transformer performance [16].

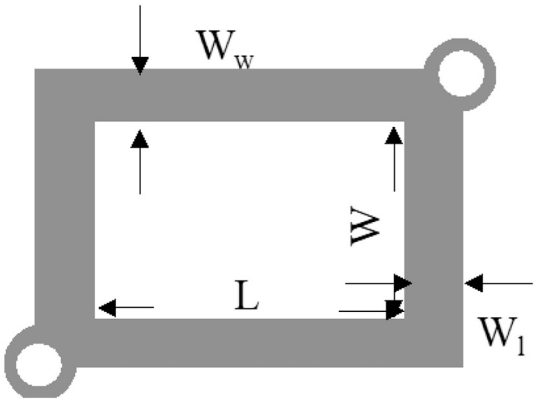

Fig. 2. Geometric definition of a lamination of the magnetic core (top view). W_w and W_l are the widths of the long and short rectangular arms, respectively, while W and L are the width and length of the inner rectangular window, respectively.

Fig. 1 shows a schematic representation of the transformers realized in this study. The magnetic core of the transformer comprises a rectangular, multilayer laminated structure, with alternating magnetic and electrical insulation layers. A top view of the geometry of a single core layer is shown in Fig. 2, with geometric parameters defined. In addition to the rectangular core, two ring-like features at opposite diagonal corners of the core are evident; these features are not intended to contribute magnetically to the core performance, but are utilized in multilayer core fabrication as will be discussed below.

Permalloy (Ni(80%)-Fe(20%)) was selected as the magnetic core material since it has both a higher saturation flux density and a higher magnetic permeability when compared to conventional ferrite materials. However, the typical drawback of magnetic metallic alloys, including NiFe, is the substantial eddy current loss that is generated during high frequency operation [32]. To minimize the eddy current loss, the core is fabricated as a stack of individual insulated laminations, in which the thickness of an individual magnetic layer in the core is on the order of, or smaller than, the magnetic skin depth at the operating frequency of interest.

For a given magnetic material, the skin depth δ_m of the core can be calculated as [33]:

$$\delta_m = \sqrt{\frac{\rho_m}{\pi f \mu_0 \mu_r}} \tag{1}$$

where ρ_m is the electrical resistivity of the core, f is the operating frequency, μ_0 is the vacuum permeability, and μ_r is the relative permeability of the core. The reported resistivity and relative permeability of electrodeposited NiFe are 2.5×10^{-7} Ω·m and 800, respectively [34]. For a nominal operation frequency of 2 MHz, the NiFe skin depth calculated from (1) is 6.3 μm. This value will be used in design of individual lamination thicknesses.

Test transformers were fabricated in accordance with five different specifications. Individual magnetic lamination thicknesses (t_{m0}) were designed up to 6 μm to examine the tradeoffs between lamination thickness and transformer performance. Referring to Fig. 2, the core window area (W·L) was designed to accommodate the total area needed for coil turns. The dimensions of the test transformers are summarized in Table 2. With the exception of transformer geometry S1, the targeted primary and secondary inductance for these transformers were above 2 μH and 200 μH, respectively, with a 10:1 secondary:primary nominal turns ratio.

Table 2
Dimensions of the fabricated test transformers.

	Magnetic Core Dimensions							
Sample no.	W (mm)	L (mm)	t_m (mm)	t_{m0} (μm)	W_w (mm)	W_l (mm)	N_p (turns)	N_s (turns)
S1	0.8	1.2	0.27	1	0.39	0.3	8	80
S2	1.2	1.2	0.24	2	0.73	0.3	12	120
S3	1.2	1.2	0.24	3	0.73	0.3	12	130
S4	1.2	1.2	0.18	3	0.73	0.3	12	130
S5	1.2	1.2	0.18	6	0.73	0.3	12	130

t_m: effective core thickness, t_{m0}: individual magnetic layer thickness, N_p: primary coil turn number, N_s: secondary coil turn number.

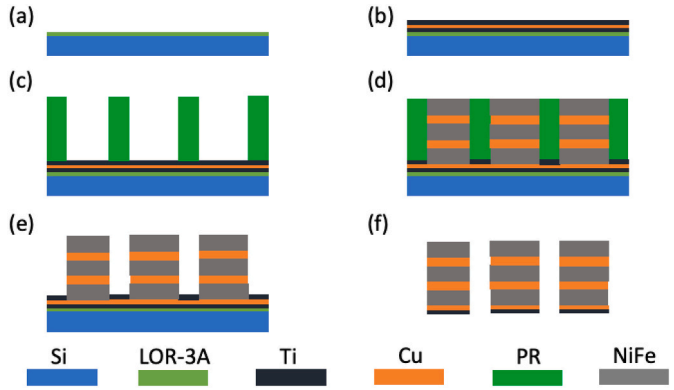

Fig. 3. Fabrication scheme of NiFe/Cu multilayer constructs. (a) deposition of lift-off resist; (b) deposition of seed layer; (c) deposition of electrpllating mold; (d) removal of uppermost seed layer; (e) sequential multilayer electrodeposition; (f) removal of the photoresist mold and LOR yielding a set of freestanding multilayer constructs.

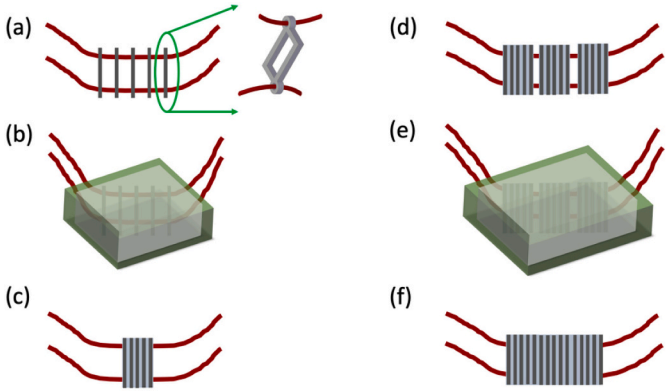

Fig. 4. Fabrication scheme of the laminated magnetic core. (a) A multilayer construct, such as one of the stacks separated from the substrate of Fig. 3f, is placed on self-assembly guide wires and immersed in selective copper etchant. Upon removal of the copper, individual laminations (as shown in the insert) are held in registration by the assembly wires. (b) The wire-supported laminations are immersed in Novec solution to coat them with fluoropolymer insulation. (c) The laminations are removed from the Novec solution and self-assemble into a core segment. (d) To form thicker cores, the multiple core segments of (c) are threaded onto assembly wires. (e) Multiple core segments are immersed in Novec solution. (f) Multiple core segments self-assemble into a full core.

3. Fabrication

The laminated magnetic core comprised alternating magnetic and electrically insulative layers. Electrodeposited NiFe permalloy was employed as the magnetic layer, while a fluorinated acrylic polymer (Novec™ 1700 Electronic Grade Coating, 3 M™Corporation) was selected as the insulation material. Novec 1700 is a solution of a 2 wt% fluorinated acrylic polymer dissolved in a hydrofluoroether solvent and commonly used in printed circuit boards and electronic components protection from moisture and corrosion [21].

The laminated magnetic core fabrication was extended from lamination processes previously reported for inductors [20,21]. The formation of thick cores is facilitated by the use of a hierarchical approach. Sequential multilayer deposition is used to create a plurality of *multilayer constructs*. Multilayer constructs are then formed into *core segments* through self-assembly. Finally, core segments themselves are further self-assembled to form thick laminated *cores* comprising a large number of thin, insulated laminations.

The fabrication of multilayer constructs is shown in Fig. 3. Photoresist LOR-3A was spin-coated on a silicon wafer to act as a sacrificial layer (Fig. 3(a)). An electrodeposition seed layer (Ti/Cu/Ti) was sputter-deposited on the LOR-3A (Fig. 3(b)). A photoresist mold in the shape of the core (Fig. 2) was then lithographically patterned on the seed layer (Fig. 3(c)). After etching the surface Ti layer, alternating sequential electrodeposition was performed within the mold using an automated robot that transferred the wafer between NiFe and copper baths until the targeted numbers and thicknesses of layers were reached (Fig. 3(d)). The desired thickness of an individual layer was achieved by adjusting the electrodeposition time. The photoresist mold was then stripped (Fig. 3 (e)). The NiFe/Cu multilayer constructs, each typically comprising between 5 and 30 layers of NiFe of desired thickness (between which are 4–29 Cu interlayers of 1 μm thickness), were then detached from the silicon substrate by dissolving the LOR photoresist (Fig. 3(f)).

Self-assembly was exploited to transform the multilayer constructs into core segments. To aid in self-assembly, strands of thin, enamel-coated copper magnet wire were strung through each of the assembly rings at the opposite diagonals of the multilayer structure. The multilayer constructs, supported by these assembly wires, were then placed in a selective copper etchant to remove the copper layers. Once the copper was removed, the NiFe layers separated from each other, but were held in registration by the assembly wires (Fig. 4(a)). To insulate the individual laminations and self-assemble the core segment, the assembly wires bearing the individual laminations were immersed in Novec 1700 solution (Fig. 4(b)). After removal from the Novec solution, and guided in part by the assembly wires, the individual lamination layers self-assembled into a single core segment due to surface tension (Fig. 4 (c)). The low viscosity and rapid drying rate of the solution facilitated the self-assembly of NiFe layers with a thin and conformal coating between the individual layers. Multiple core segments could then be further assembled into thicker cores by repeating the previous procedure, but self-assembling segments rather than laminations. (Fig. 4(d)–(f)). More details describing the self-assembly process can be found in [35].

Fig. 5(a) shows a fabricated magnetic core realized using the above process. Geometric design S5 is used here as an example. The core was assembled using six stacks of multilayer constructs; each construct comprised 5 layers of NiFe, each of which was 6 μm in thickness. The final core therefore comprises 30 layers of NiFe with a magnetic thickness of 180 μm. The total thickness of the core, however, is 335 μm. It should be noted that this total thickness includes not only the magnetic lamination thickness and the interlayer insulation thickness, but also

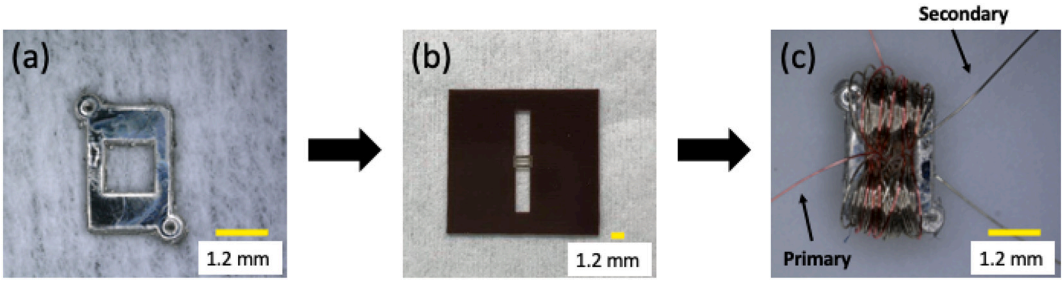

Fig. 5. Fabricated magnetic cores and transformer winding. Transformer S5 is shown as an example. (a) Laminated magnetic core produced as described in Figs. 3 and 4 after assembly. (b) Laminated magnetic core placed on a laser-machined polyester shim which will be used as a winding aid. (c) A 12:130 turn transformer wound on the laminated magnetic core.

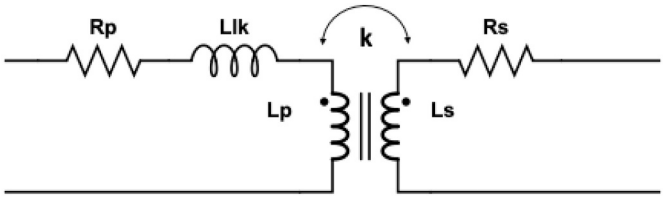

Fig. 6. Equivalent circuit model of the transformer.

stacking inefficiencies due to nonuniformity in layer thickness (discussed below).

Transformers were fabricated by manually winding coils on the self-assembled laminated magnetic cores. To aid in winding, a polyester shim was machined using a CO_2 laser to form a rectangular window in the middle of the shim that had the same width as that of the core. The core was attached to the shim with core window aligned to the shim window (Fig. 5(b)). Enamel-coated magnet wire was hand wound on the top and bottom sides of the core, with the same number of turns on each side, to form the secondary coil. Specifically, the coils were wound in a multi-level fashion with the same number of turns on an individual level. The primary coil was then wound on top of the secondary coil. The transformer was then detached from the polyester shim (Fig. 5(c)).

The turn design of transformer windings for the five transformers are given in Table 2. A variety of wire types were used in transformer winding. Transformer S1 used 45-gauge copper magnet wire for the primary and secondary. Transformers S2-S4 used 45-gauge aluminum magnet wire to minimize coil weight. Transformer S5 used a 45-gauge copper primary winding and a 45-gauge aluminum secondary winding, in recognition that in step-up configurations primary currents would typically exceed secondary currents; this approach still allowed the high turn count secondary winding to benefit from the lower mass density of aluminum wire compared to copper.

4. Characterization

Transformers will typically be used at frequencies below their self-resonant frequency. In this frequency range, parasitic capacitances can be neglected, and the equivalent circuit model for the transformer can be expressed as shown in Fig. 6. In this simplified model, the parameters of interest are the primary resistance R_p and inductance L_p; the secondary resistance R_s and inductance L_s, and the primary-to-secondary coupling coefficient k. In addition to these operational parameters, the resonant frequency itself was also experimentally determined.

The inductance and resistance of the fabricated transformers were measured in the frequency range of 50 kHz-100 MHz using a network analyzer. Table 3 shows the primary and secondary inductance of the fabricated transformers of the geometries detailed in Table 2 as a function of frequency. In general, the transformers exhibited high primary and secondary inductance values. It was noted that these values were generally maintained up to their resonance frequencies in the MHz range, suggestive of eddy current loss suppression and thus good insulation between magnetic layers in the cores.

At a frequency of 50 kHz, the inductances of the transformer primaries varied from 0.66 μH to 2.96 μH, and the inductances of the transformer secondaries varied from 67 μH to 312 μH. The inductance of transformer S5 at 1 MHz was slightly reduced, which is attributed to increased core loss of this sample. Transformer S3 exhibited the highest inductance both on the primary and secondary sides, consistent with its largest effective core volume. On the other hand, transformer S1 had the lowest inductance on both sides because of its smallest core and fewest coil turns. In ideal cases, the inductance ratio between primary and secondary should be the square of the turns ratio. However, in our cases, the inductance ratio was slightly smaller than the square of the turns ratio, attributable to magnetic coupling of less than unity in these small devices.

The effective relative permeability of the laminated magnetic cores in transformers listed in Table 2 were calculated using the following equation:

$$\mu_r = \frac{Ll}{\mu_0 N^2 A} \tag{2}$$

where L is the inductance of the transformer, l is the length of the closed magnetic path and is the middle line between the outer and inner perimeters, μ_0 is the vacuum permeability, N is the number of coil turns, and A is the magnetic cross-sectional area of the core, i.e., the

Table 3
Inductance and resistance of the transformers.

Sample no.	L_p at 50 kHz (μH)	L_s at 50 kHz (μH)	L_p at 1 MHz (μH)	L_s at 1 MHz (μH)	R_p at 50 kHz (Ω)	R_s at 50 kHz (Ω)	R_p at 1 MHz (Ω)	R_s at 1 MHz (Ω)	f_{0p} (MHz)	f_{0s} (MHz)
S1	0.66	67	0.66	60	1.2	4.7	1.4	21	4.6	5.6
S2	2	175	2.02	180	9	10	12	137	3.1	4.4
S3	2.96	312	3.34	273	4.3	33	6.5	179	2.6	3.9
S4	1.95	198	1.97	200	3.6	32	4.9	144	2.9	3.7
S5	2.75	253	2.2	234	1.6	13	5.4	369	2.6	3.5

L_p: primary inductance, L_s: secondary inductance, R_p: primary resistance, R_s: secondary resistance, f_{0p}: primary self-resonance frequency, f_{0s}: secondary self-resonance frequency.

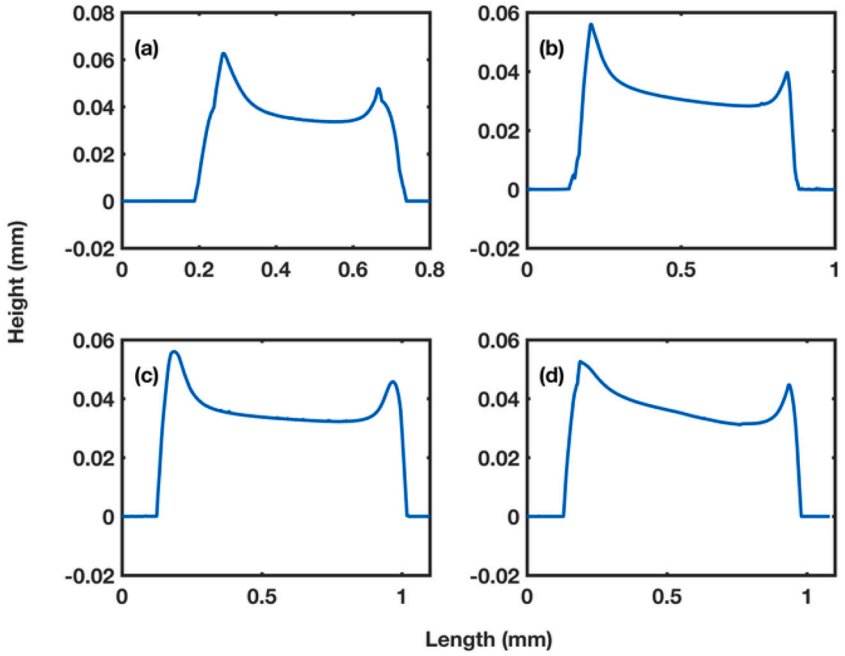

Fig. 7. Height versus width (W_w) of various NiFe/Cu multilayer constructs as measured by surface profilometry. (a) NiFe - 30 layers of 1 μm; Cu - 29layers of 1 μm. (b) NiFe - 15 layers of 2 μm; Cu - 14 layers of 1 μm. (c) NiFe – 10 layers of 3 μm; Cu - 9 layers of 1 μm. (d) NiFe – 5 layers of 6 μm; Cu – 4 layers of 1 μm. Note that the vertical scale of these figures is exaggerated by approximately a factor of 20.

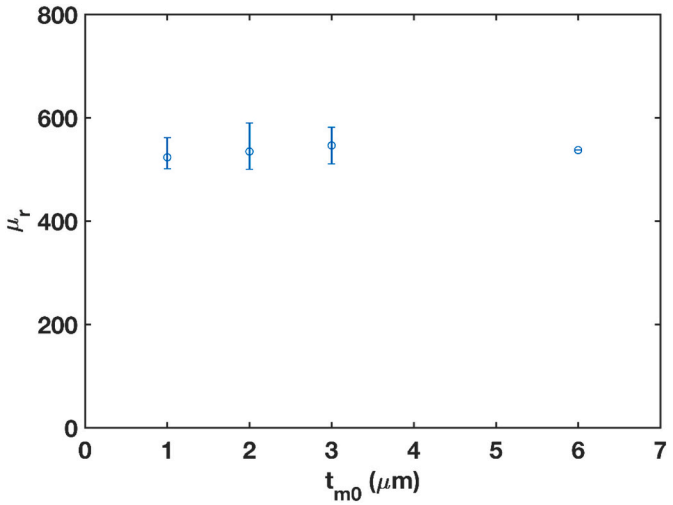

Fig. 8. Calculated effective relative permeability of the laminated magnetic core as a function of individual magnetic layer thickness. Error bars mean the maximum and minimum values of the data points.

summation of the cross-sectional areas of the NiFe layers. This effective cross-sectional area was calculated by measuring the thickness of the NiFe/Cu multilayer structures. Fig. 7 shows the thickness profiles of electroplated constructs as a function of construct width (W_w). Substantial nonuniformity at the edges of the electrodeposited structure were observed. Such behavior has been observed previously. One model discussing this phenomenon is the fluidic friction model developed by Luo et al [36]. In brief, the ion concentration at the edge was higher than that of the center due to formation of a boundary layer at the edge by fluid friction, which could result in more rapid plating at the edge of the mold.

To analyze the transformer performance, the cross-sectional area of the NiFe portion of the multilayer construct was extracted by integrating the measured width-thickness curves and taking fractions based on the NiFe nominal thickness. The effective cross-sectional area was calculated by multiplying the cross-sectional area of the NiFe portion of the multilayer construct by the number of multilayers. Based on this area, together with the measured inductance results, Eq. (2) was used to extract the relative permeability of the cores. Fig. 8 shows the core relative permeability plotted as a function of multilayer thickness. The effective relative permeability in these constructs was close to 600, in reasonable agreement with previously reported values, and did not change significantly with increasing individual magnetic layer thickness.

Table 3 also shows the primary and secondary resistance of the fabricated transformers listed in Table 2 as a function of frequency. The resistance values of fabricated transformers were varied from 1.2 Ω to 9 Ω for primary coils and 4.7 Ω to 33 Ω for secondary coils at 50 kHz. For S1 and the primary of S5, the resistance at low frequency mainly came from the winding. For S1, the primary coil was 100 mm long (20 mm for turns and 80 mm for leads); the secondary coil was 280 mm long (200 mm for turns and 80 mm for leads). The resistance of the 45-gauge copper magnet wire was 10.4 Ω/m. Thus, the calculated primary and secondary resistances were 1 Ω and 3 Ω, respectively, close to the measured values. For S5, the primary coil was 107 mm long (27 mm for turns and 80 mm for leads), and the calculated primary resistance was 1.1 Ω, also close to the measured value. For S2-S4 and the secondary of S5, the resistance at low frequency came from the winding as well as connection between winding and measurement-use thick wires since these devices used aluminum windings with unsatisfactory solderability. As the frequency gradually increased (at 1 MHz), other effects such as core loss and self-resonance started to play a role in the resistance. All transformers showed increases in resistance at 1 MHz. However, transformer S5 showed a relatively high increase rate, suggesting that core loss might have been more of a factor with this device.

The transformer coupling coefficient is a critical parameter that characterizes its energy transfer performance [30]. The coupling coefficient (k) was determined using the following equation [37]:

$$k = \sqrt{1 - \frac{L_{leak}}{L_{pri}}} \tag{3}$$

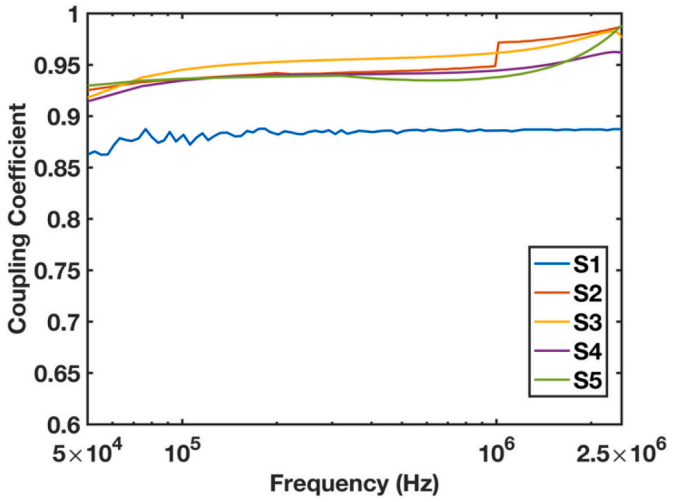

Fig. 9. Coupling coefficient of the fabricated transformers as a function of frequency.

where L_{leak} is the primary leakage inductance and L_{pri} is the primary inductance of the transformer. The primary inductance was determined by measuring the inductance of the primary coil with the secondary coil open, while the leakage inductance was determined by measuring the primary inductance when the secondary coil was shorted. Overall, the transformers exhibited strong magnetic coupling, due to the closed magnetic core design and high permeability of the core. Fig. 9 shows the coupling coefficient of the fabricated transformers listed in Table 2 as a function of frequency. With the exception of transformer S1, all transformers exhibited coupling coefficients of 0.9–0.95 in frequency ranges of interest.

Fig. 10 shows the voltage step-up testing setup of the transformer as well as the circuit diagram of connections for the device under test. The primary coil of the transformer was connected to a function generator. R_s represents the internal impedance of the function generator. The primary and secondary coils were connected to an oscilloscope to measure the primary and secondary voltage respectively. We measured the voltages in the time domain to ensure the voltage in primary and secondary maintained appropriate phase relationships. All voltages maintained their expected phase relationships below resonance. Because of this time domain measurement, voltages are given below as peak-to-peak measurements. Conversion to other values such as RMS are straightforward, as the measurements indicated a sinusoidal response as expected.

Fig. 11 shows the voltage step-up ratio of the transformer S2 as a function of frequency. The step-up ratio was the voltage ratio of secondary to primary coils measured under an input of 1 V peak sinusoidal excitation. The theoretical step-up ratio is equal to the ratio of secondary to primary winding turns; this was 10:1 for transformer S2. The measured step-up ratio was 7.8 at 0.4 MHz and increased to 10 at 1.6 MHz. With a primary voltage of 3.8 V peak to peak, a secondary voltage of 34.6 V peak to peak was observed. Even though the saturation current of the transformers was not measured, the calculated value for the

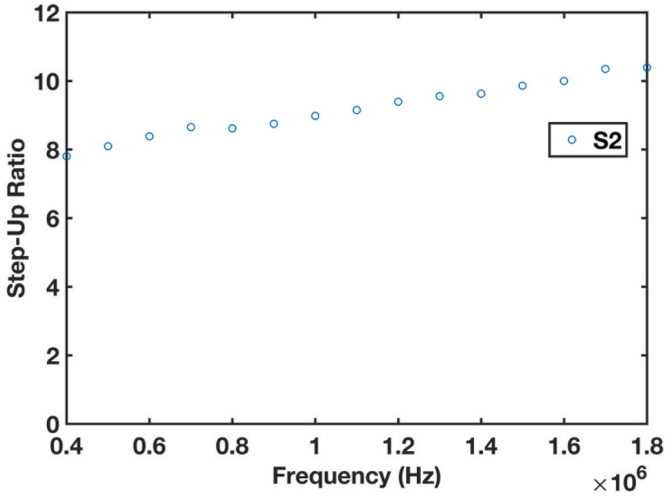

Fig. 11. Voltage step-up ratio of the transformer S2 as a function of frequency.

Table 4
Volume and weight of the transformers and commercial coupled inductors.

Sample no.	Volume (mm^3)	L_p per volume ($\mu H/mm^3$)	Weight (mg)	L_p per weight ($\mu H/mg$)
S1	2.3	0.29	11.9	0.05
S2	3.35	0.6	11.75	0.17
S3	3.6	0.82	13.22	0.22
S4	3.11	0.63	11	0.17
S5	2.97	0.93	11.68	0.23
Commercial device				
LPR4012-202LMR_	21.29	0.09	60	0.03

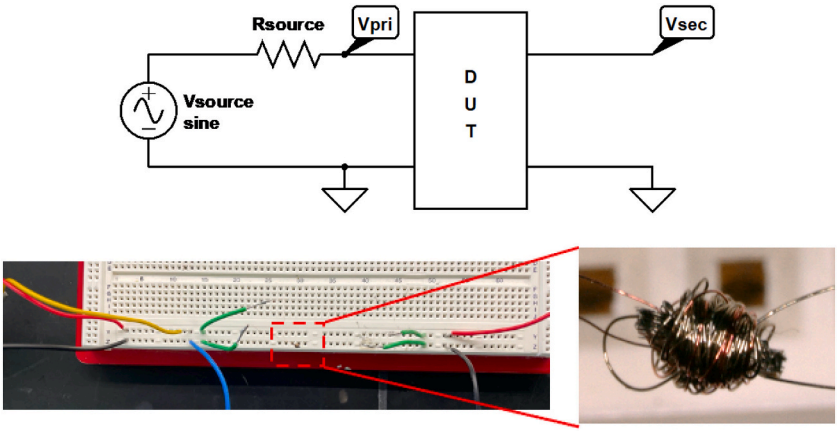

Fig. 10. Schematic and photograph of transformers under test. (Top) the transformer, denoted DUT, has its primary connected to a variable-frequency sinusoidal voltage source of magnitude Vsource, with internal source resistance Rsource. Both the voltage at the input of the DUT (Vpri) and at the output (Vsec) are measured using an oscilloscope. (Bottom) Photograph of the DUT shown in a standard protoboard.

primary winding based on the saturation flux density of permalloy was 0.75–1.06 A. The step-up ratio of other transformers showed similar trends to that of transformer S2.

Table 4 shows the measured volume of the fabricated transformers compared to commercial coupled inductors. Transformer S1 had the smallest size because it had the smallest core footprint area and fewest coil turns. However, it was not lighter than other devices because it used copper wires for coils. Transformer S3 was larger and heavier than S2 because it had more secondary turns. Transformers S4 and S5 were smaller and lighter than S3 because they had less magnetic layers. Transformer S5 was smaller than S4 because it had less insulation layers. However, it was slightly heavier because its primary coil was copper.

The fabricated devices were compared to a commercial transformer with similar primary inductance and turns ratio. Transformer LPR4012-202LMR_ had a primary inductance of 2 μH and 1:10 turns ratio. It shows that our fabricated devices were 7 times smaller and 5 times lighter than the commercial devices, resulting in a 7 times higher inductance per volume as well as 5 times higher inductance per weight.

Since the saturation current of the transformers is on the order of 1A, these transformers will have application in higher voltage, lower current scenarios where compactness is of importance. For instance, Choi et al. proposed an optimized power management integrated circuit for an envelope tracking power amplifier in handsets [38]. The current in the supply modulator was less than 1 A. In addition, the transformers can potentially be used in energy harvesting for dielectric elastomer actuators. For example, Zhao et al. proposed a wearable haptic communication device based on dielectric elastomer actuators [39]. High voltage was required for actuation while current was limited to 0.2 mA to ensure human safety. These and other scenarios where compact high voltage conversion may be required are of particular interest for this technology.

5. Conclusion

Closed magnetic core, high turns ratio step-up transformers utilizing laminated permalloy cores were developed and characterized in the MHz operating frequency range. The magnetic core thickness of the transformers was varied from 0.18 to 0.27 mm. The number of primary and secondary turns were varied from 8 to 12 and 80 to 130, respectively. With various designs, the transformers had primary inductance of 0.66–2.96 μH and secondary inductance of 67–312 μH, which can be maintained up to their self-resonance in the MHz range of frequency. The transformers had primary resistance of 1.2–9 Ω and secondary resistance of 4.7–33 Ω at 50 kHz. The coupling coefficient of the transformers was above 0.85 and the step-up ratio can achieve the theoretical value. The transformers had estimated saturation current of 0.75–1.06 A. The fabricated transformers showed 7 times higher inductance per volume and 5 times higher inductance per weight compared to commercial coupled inductors, demonstrating promise for their use in ultracompact magnetic systems.

Declaration of Competing Interest

The authors declare that they have no known competing financial interests or personal relationships that could have appeared to influence the work reported in this paper.

Acknowledgements

This work was supported by the Defense Advanced Research Projects Agency, contract number HR0011-19-C-0039, under the supervision of Dr. R. Polcawich. Microfabrication took place in the Singh Center for Nanotechnology at the University of Pennsylvania, which is supported by the NSF National Nanotechnology Coordinated Infrastructure Program under grant NNCI-2025608. Technical discussions with Dr. Minsoo Kim of Apple are gratefully acknowledged.

References

[1] Q. Li, M. Lim, J. Sun, A. Ball, Y. Ying, F.C. Lee, K.D.T. Ngo, Technology road map for high frequency integrated DC-DC converter, in: Conference Proceedings - IEEE Applied Power Electronics Conference and Exposition, APEC, 2010, pp. 533–539, https://doi.org/10.1109/APEC.2010.5433619.

[2] C.R. Sullivan, D.V. Harburg, J. Qiu, C.G. Levey, D. Yao, Integrating magnetics for on-chip power: a perspective, in: IEEE Transactions on Power Electronics 28, 2013, pp. 4342–4353, https://doi.org/10.1109/TPEL.2013.2240465.

[3] F. Waldron, R. Foley, J. Slowey, A.N. Alderman, B.C. Narveson, S.C.Ó. Mathúna, Technology roadmapping for power supply in package (PSiP) and power supply on chip (PwrSoC), in: IEEE Transactions on Power Electronics 28, 2013, pp. 4137–4145, https://doi.org/10.1109/TPEL.2012.2227821.

[4] M. Qiao, L. Liang, J. Zu, D. Hou, Z. Li, B. Zhang, A review of high-voltage integrated power device for AC/DC switching application, Microelectron. Eng. 232 (2020), https://doi.org/10.1016/j.mee.2020.111416.

[5] S. Abdelnasser, M.A. Sakr, M. Serry, Nanostructured graphene-platinum-PEDOT electrode materials for enhanced Schottky performance and power conversion applications, Microelectron. Eng. 216 (2019), https://doi.org/10.1016/j.mee.2019.111045.

[6] A.W. Lotfi, M.A. Wilkowski, Issues and Advances in High-Frequency Magnetics for Switching Power Supplies, n.d.

[7] J. Kim, M. Kim, F. Herrault, J.Y. Park, M.G. Allen, Electrodeposited nanolaminated conife cores for ultracompact DC-DC power conversion, IEEE Trans. Power Electron. 30 (2015) 5078–5087, https://doi.org/10.1109/TPEL.2014.2368140.

[8] A. AL-Osta, B.S. Samer, U.T. Nakate, V.V. Jadhav, R.S. Mane, Electrodeposited spruce leaf-like structured copper bismuth oxide electrode for supercapacitor application, Microelectron. Eng. 229 (2020), https://doi.org/10.1016/j.mee.2020.111359.

[9] H.C. Baelhadj, S.S. Adhikari, H. Davoodi, V. Badilita, M.İ. Beyaz, A sub-cm3 energy harvester for in-vivo biosensors, Microelectron. Eng. 226 (2020), https://doi.org/10.1016/j.mee.2020.111288.

[10] M. Aleksandrova, Polymeric seed layer as a simple approach for nanostructuring of Ga-doped ZnO films for flexible piezoelectric energy harvesting, Microelectron. Eng. 233 (2020), https://doi.org/10.1016/j.mee.2020.111434.

[11] D.J. Perreault, J. Hu, J.M. Rivasy, Y. Han, O. Leitermann, R.C.N. Pilawa-Podgurski, A. Sagneri, C.R. Sullivan, Opportunities and challenges in very high frequency power conversion, in: Conference Proceedings - IEEE Applied Power Electronics Conference and Exposition, APEC, 2009, pp. 1–14, https://doi.org/10.1109/APEC.2009.4802625.

[12] C.Ó. Mathúna, N. Wang, S. Kulkarni, S. Roy, Review of integrated magnetics for power supply on chip (PwrSoC), IEEE Trans. Power Electron. 27 (2012) 4799–4816, https://doi.org/10.1109/TPEL.2012.2198891.

[13] J. Kim, J.K. Kim, M. Kim, F. Herrault, M.G. Allen, Microfabrication of toroidal inductors integrated with nanolaminated ferromagnetic metallic cores, J. Micromech. Microeng. 23 (2013), https://doi.org/10.1088/0960-1317/23/11/114006.

[14] F. Herrault, S. Cui, X.N. Guan, A.F. Gross, Synthesis and binder-free assembly of SrFe12O19 nano-platelets for wafer-scale patterning of magnetic components, Microelectron. Eng. 236 (2021), https://doi.org/10.1016/j.mee.2020.111467.

[15] J.W. Park, F. Cros, M.G. Allen, Planar spiral inductors with multilayer micrometer-scale laminated cores for compact-packaging power converter applications, in: IEEE Transactions on Magnetics, 2004, pp. 2020–2022, https://doi.org/10.1109/TMAG.2004.832159.

[16] E.J. Yun, M. Jung, C. Il Cheon, H.G. Nam, Microfabrication and characteristics of low-power high-performance magnetic thin-film transformers, in: IEEE Transactions on Magnetics 40, 2004, pp. 65–70, https://doi.org/10.1109/TMAG.2003.821119.

[17] M. Mino, T. Yachi, A. Tago, K. Yanagisawa, K. Sakakibara, A New Planar Microtransformer for Use in Micro-Switching Converters, 1992.

[18] D.S. Gardner, G. Schrom, P. Hazucha, F. Paillet, T. Karnik, S. Borkar, J. Saulters, J. Owens, J. Wetzel, Integrated on-chip inductors with magnetic films, in: Technical Digest - International Electron Devices Meeting, IEDM, 2006, https://doi.org/10.1109/IEDM.2006.347002.

[19] K. Ikeda, K. Kobayashi, M. Fujimoto, Multilayer nanogranular magnetic thin films for GHz applications, J. Appl. Phys. 92 (2002) 5395–5400, https://doi.org/10.1063/1.1510562.

[20] J. Kim, M. Kim, P. Galle, F. Herrault, R. Shafer, J.Y. Park, M.G. Allen, Nanolaminated permalloy core for high-flux, high-frequency ultracompact power conversion, IEEE Trans. Power Electron. 28 (2013) 4376–4383, https://doi.org/10.1109/TPEL.2013.2238639.

[21] J. Kim, M.G. Allen, Nanolaminated CoNiFe cores with dip-coated fluoroacrylic polymer interlamination insulation: fabrication, electrical characterization, and performance reliability, in: Proceedings - Electronic Components and Technology Conference, Institute of Electrical and Electronics Engineers Inc., 2017, pp. 798–803, https://doi.org/10.1109/ECTC.2017.197.

[22] S. Bae, Y.K. Hong, J.J. Lee, J. Jalli, G.S. Abo, A. Lyle, B.C. Choi, G.W. Donohoe, High Q Ni-Zn-Cu Ferrite inductor for on-chip power module, in: IEEE Transactions on Magnetics, 2009, pp. 4773–4776, https://doi.org/10.1109/TMAG.2009.2023856.

[23] I. Kowase, T. Sato, K. Yamasawa, Y. Miura, A planar inductor using Mn-Zn ferrite/polyimide composite thick film for low-voltage and large-current dc-dc converter, in: IEEE Transactions on Magnetics, 2005, pp. 3991–3993, https://doi.org/10.1109/TMAG.2005.855164.

[24] Y. Fukuda, T. Inoue, T. Mizoguchi, S. Yatabe, Y. Tachi, Planar inductor with ferrite layers for DC-DC converter, IEEE Trans. Magn. 39 (2003) 2057–2061, https://doi.org/10.1109/TMAG.2003.812708.
[25] D. Flynn, A. Toon, L. Allen, R. Dhariwal, M.P.Y. Desmulliez, Characterization of core materials for microscale magnetic components operating in the megahertz frequency range, IEEE Trans. Magn. 43 (2007) 3171–3180, https://doi.org/10.1109/TMAG.2007.895700.
[26] W.P. Taylor, M. Schneider, H. Baltes, M.G. Allen, A NiFeMo Electroplating Bath for Micromachined Structures, 1999.
[27] D. Flynn, R.S. Dhariwal, M.P.Y. Desmulliez, A design study of microscale magnetic components for operation in the MHz frequency range, J. Micromech. Microeng. 16 (2006) 1811–1818, https://doi.org/10.1088/0960-1317/16/9/008.
[28] R. Meere, T. O'Donnell, H.J. Bergveld, N. Wang, S.C. O'Mathuna, Analysis of microinductor performance in a 20–100 MHz DC/DC converter, IEEE Trans. Power Electron. 24 (2009) 2212–2218, https://doi.org/10.1109/TPEL.2009.2021942.
[29] T. el Mastouli, J.P. Laur, J.L. Sanchez, M. Brunet, D. Bourrier, M. Dilhan, Micro-inductors integrated on silicon for DC-DC converters, in: Micromachining and Microfabrication Process Technology XIII, SPIE, 2008, p. 68820A, https://doi.org/10.1117/12.763085.
[30] X. Xing, N.X. Sun, B. Chen, High-bandwidth low-insertion loss solenoid transformers using FeCoB multilayers, IEEE Trans. Power Electron. 28 (2013) 4395–4401, https://doi.org/10.1109/TPEL.2012.2233759.
[31] L. Wang, J. Xie, A. Su, Monolithic Fabrication of Electroplated Solenoid Inductors Using Three-Dimensional Photolithography of a Thick Photoresist Related Content High-frequency Magnetic Properties of [Fe 80 Ni 20-O/SiO 2] n Multilayer Film Served as Magnetic Core of Solenoid Inductor, 1998.
[32] J.-W. Park, J.Y. Park, Y.-H. Joung, M.G. Allen, Fabrication of High Current and Low Profile Micromachined Inductor With Laminated Ni/Fe Core, 2002.
[33] B.D. Cullity, C.D. Graham, Introduction to Magnetic Materials Second Edition, n.d.
[34] M. Xu, T.M. Liakopoulos, C.H. Ahn, S.H. Han, H.J. Kim, A Microfabricated Transformer for High-Frequency Power or Signal Conversion, 1998.
[35] J. Kim, M. Kim, M.G. Allen, Surface tension-driven assembly of metallic nanosheets at the liquid-air interface: application to highly laminated magnetic cores, in: 2015 Transducers - 2015 18th International Conference on Solid-State Sensors, Actuators and Microsystems, Transducers 2015, Institute of Electrical and Electronics Engineers Inc., 2015, pp. 2224–2227, https://doi.org/10.1109/TRANSDUCERS.2015.7181403.
[36] J.D. Li, P. Zhang, Y.H. Wu, Y.S. Liu, M. Xuan, Uniformity study of nickel thin-film microstructure deposited by electroplating, Microsyst. Technol. 15 (2009) 505–510, https://doi.org/10.1007/s00542-008-0754-5.
[37] Y. Gao, S. Zare, X.J. Yang, T.X. Nan, Z.Y. Zhou, M. Onabajo, K.P. O'Brien, U. Jalan, M. Ei-Tatani, P. Fisher, M. Liu, A. Aronow, K. Mahalingam, B.M. Howe, G.J. Brown, N.X. Sun, High quality factor integrated gigahertz magnetic transformers with FeGaB/Al2O3 multilayer films for radio frequency integrated circuits applications, J. Appl. Phys. (2014), https://doi.org/10.1063/1.4868622. American Institute of Physics Inc.
[38] J. Choi, D. Kim, D. Kang, B. Kim, A new power management IC architecture for envelope tracking power amplifier, IEEE Trans. Microwave Theor. Techniques 59 (2011) 1796–1802, https://doi.org/10.1109/TMTT.2011.2134108.
[39] H. Zhao, A.M. Hussain, A. Israr, D.M. Vogt, M. Duduta, D.R. Clarke, R.J. Wood, A wearable soft haptic communicator based on dielectric elastomer actuators, Soft Robot. 7 (2020) 451–461, https://doi.org/10.1089/soro.2019.0113.